UWB Positioning with Virtual Anchors and Floor Plan Information

Paul Meissner*, Christoph Steiner** and Klaus Witrisal*
*Graz University of Technology, Graz, Austria, Email: {paul.meissner, witrisal}@tugraz.at
**Communication Technology Laboratory, ETH Zurich, Email: steinech@nari.ee.ethz.ch

***Abstract*—This paper describes an indoor positioning method using ultra-wideband (UWB) signals from one single transmitter at a known location together with a-priori floor plan information. The position of the receiver is estimated from the signal reflections in the room walls and the direct signal path. Therefore, the algorithm is inherently robust to non-line-of-sight conditions, which are considered a key problem in range-based positioning. We introduce likelihood models for the individual range measurements that correspond to single and double reflections. Using the room geometry, these reflections can be mapped to virtual anchors at known positions and the multilateration problem can be solved using statistical techniques. Simulation results show that this approach of position estimation is a promising candidate for robust and accurate localization.**

I. Introduction

Indoor localization is a research topic that has received a high amount of attention over the last years. Potential applications include position tracking for maintenance workers or rescue forces in emergency scenarios. An often adapted method is multilateration based on radio signals. Here, range estimates to multiple nodes at known locations, called anchors, are used to estimate the unknown position of a node. For two-dimensional positioning, the range measurements to at least three anchors are needed. However, such positioning systems are error-prone in non-line-of-sight (NLOS) conditions, which cause biased range estimates [1]. There are numerous approaches to detect whether one or more anchors are in an NLOS condition, such that their range information can be discarded. Such approaches can use decision theory [2], [3] or neural networks [4], for example. Few works actually try to exploit the signal energy that is received over those indirect transmission paths. In [5] for example, reflected signals are used to build a map of an indoor location.

In this paper, we introduce an indoor positioning algorithm that makes use of the reflections of a transmitted ultra-wideband (UWB) signal together with given floor plan information. Using this algorithm, the unknown position of a node can be estimated with just one reference node that is at a fixed and known location. The receiver uses single and double reflections of the transmitted signal in the room walls. Through the use of UWB signals, these reflections are resolvable at the receiver [6], [7]. Using the known room geometry, the set of reflections is mapped onto a set of *virtual anchors* (VAs), i.e., the known positions of virtual sources that can be used for estimating the position of the receiver.

We explicitly omit the step of extracting the ranges to the virtual sources from the channel impulse response (CIR) and focus on an investigation of the positioning algorithm. This approach is taken in order to show the general applicability of the algorithm as a first step. This is also motivated by [8], where it is shown that the task of optimal postion estimation based on received signals can be split up in the two subtasks of maximum-likelihood estimation of intermediate parameters and subsequently the ML or MAP estimation of the location. ML estimation of the deterministic multipath components could be done by a modified SAGE- or CLEAN-algorithm, for example [9], [10].

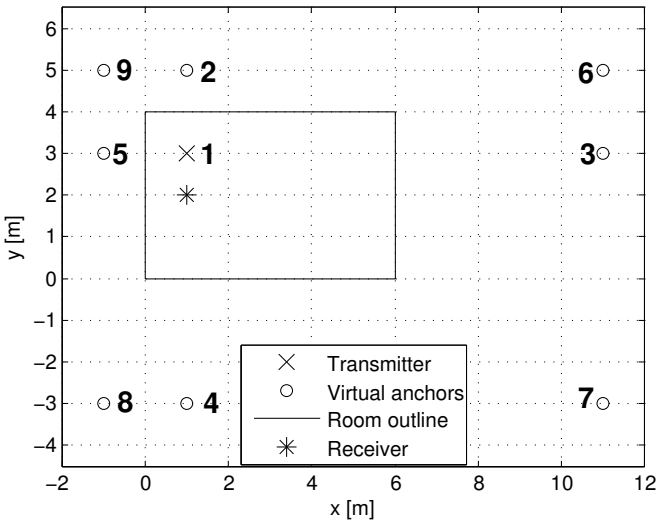

Fig. 1. Scenario and geometry used in the positioning problem. The circles correspond to the position of virtual anchors, that are the computed positions of the hypothetical sources of single and double reflections of the transmitter's signal in the room walls.

This paper is organized as follows: Section II contains an overview over the positioning problem and our proposed solution, Section III introduces the statistical models that are used, Section IV provides simulation results of the performance and Section V draws conclusions and discusses future research planned on this topic.

II. Problem definition and positioning algorithm

A. Prior knowledge and geometry

Fig. 1 shows the geometry that is used in the positioning problem addressed in this paper. The room is a simple

rectangular room and its geometry is assumed to be known. Within the room, there is a transmitter at a fixed and known location and a receiver, whose position is to be estimated. An algorithm for two-dimensional range-based positioning needs the distances to at least three anchor nodes with known positions, hence signals additional to the transmitter's direct path signal are needed.

Assuming that the transmitter uses an impulse-radio like signal with an ultrawide bandwidth, the measured impulse response [7] within the room contains deterministic components that correspond to reflections. In this paper, we will consider single and double reflections of the transmitter's signal in the room walls. From the receiver's perspective, these reflections can be treated equivalently as signals coming from point sources located outside of the room. The circles in Fig. 1 represent those mirror images of the transmitter. As their position can be computed using the known geometry and the known position of the transmitter, we call them *virtual anchors* (VAs).

Some of the reflected paths, as well as the direct path, could of course be obstructed. So in general, only a subset of the VAs and the transmitter itself will be available for the positioning algorithm. These imperfections and their consideration will be discussed next. We start with an outline of the overall positioning algorithm.

B. Positioning algorithm

The first step in the positioning algorithm is the computation of the VAs based on the known geometry. Assuming that a certain VA is visible (in the sense of delivering "sufficient" received signal strength) at the receiver, we expect a deterministic signal component in the channel impulse response (CIR) at a delay corresponding to the distance d_k to that image. The vector of distances from the receiver (at position $\mathbf{p}_{\mathrm{true}}$) to all the K VAs (each at position $\mathbf{p}_k$) is given as

$$\begin{aligned} \mathbf{d} &= \left[||\mathbf{p}_{\mathrm{true}} - \mathbf{p}_1||, ..., ||\mathbf{p}_{\mathrm{true}} - \mathbf{p}_K||\right]^T && (1) \\ &= [d_1, ..., d_K]^T && (2) \end{aligned}$$

where $[\cdot]^T$ denotes transposition. Let us assume that we have the ability to extract deterministic multipath components (MPCs) from the CIR. Modifications of existing algorithms like SAGE or CLEAN and their extensions to UWB (see [9], [10]) could be employed for this task. Such an MPC extraction yields a vector of range estimates to the K VAs

$$\mathbf{r} = [r_1, ..., r_K]^T \tag{3}$$

This of course assumes that all the K images are visible at the observation time and that the mapping of extracted ranges and VAs is available. Each r_k will be a noisy observation of the corresponding d_k. This noise is modeled as Gaussian, hence the r_k follow a Normal distribution

$$r_k \sim \mathcal{N}(d_k, \sigma_k^2) \tag{4}$$

We can introduce a multivariate likelihood function of the range observation vector, $p_{\mathbf{r}|\mathbf{p}}(\mathbf{r}|\mathbf{p})$, which is parametrized by the unknown position $\mathbf{p}$. Assuming that the individual entries of the vector $\mathbf{r}$ are independent, this function can be expressed as

$$\begin{aligned} p_{\mathbf{r}|\mathbf{p}}(\mathbf{r}|\mathbf{p}) &= \prod_{k=1}^{K} p_{r_k|\mathbf{p}}(r_k|\mathbf{p}) && (5) \\ &= \frac{1}{(2\pi)^{K/2}} \prod_{k=1}^{K} \frac{1}{\sigma_k} \exp\left\{-\frac{1}{2\sigma_k^2}\left[r_k - ||\mathbf{p} - \mathbf{p}_k||\right]\right\} \end{aligned}$$

A maximization of this function with respect to $\mathbf{p}$ yields a maximum likelihood estimate of the position

$$\begin{aligned} \hat{\mathbf{p}}_{\mathrm{ML}} &= \arg\max_{\mathbf{p}} p_{\mathbf{r}|\mathbf{p}}(\mathbf{r}|\mathbf{p}) && (6) \\ &= \arg\min_{\mathbf{p}} \sum_{k=1}^{K} \frac{1}{\sigma_k^2}\left[r_k - ||\mathbf{p} - \mathbf{p}_k||\right]^2 && (7) \end{aligned}$$

In practice, some of the paths to the K VAs will likely be obstructed. Therefore, the estimator in (6) is a hypothetical one. We will however use it as an upper bound in performance simulations, where it will be denoted as the *gold standard* estimator $\hat{\mathbf{p}}_{\mathrm{GS}}$. A slightly more realistic estimator is obtained if we take the visibility probability of the VAs into account and define a vector $\tilde{\mathbf{r}}$ that only contains the range estimates to the $K_{\mathrm{vis}} \leq K$ visible VAs

$$\tilde{\mathbf{r}} = [r_1, ..., r_{K_{\mathrm{vis}}}]^T \tag{8}$$

An ML estimator of the position based on $\tilde{\mathbf{r}}$ can then be found using (6), just with $\tilde{\mathbf{r}}$ as the argument of the joint likelihood function. However, this estimator is still too optimistic, as it knows the mapping of the components of the measurement vector to the visible VAs. We will therefore also just use it as a performance bound and refer to it as the *silver standard* estimator $\hat{\mathbf{p}}_{\mathrm{SS}}$. Hence, the silver standard position estimator is comparable to a conventional positioning algorithm that estimates the position from K_{vis} range estimates.

In a practical localization system based on the proposed concept, we have to face the imperfections of the MPC extraction process:

- Some of the K paths are not detected, which is caused by either obstruction of the VA or misses in the detection algorithm.
- Some spurious MPCs (not matched to an image) end up in the measurement vector because of false positive detections.
- We do not assume that the extracted ranges are in the correct order, i.e. the observed ranges are not mapped to the K_{vis} visible VAs.

This means that neither the vector $\mathbf{r}$ nor $\tilde{\mathbf{r}}$ will be available for the positioning algorithm. Instead, we consider the vector $\mathbf{z}$, that contains N range estimates extracted from the CIR

$$\mathbf{z} = [z_1, ..., z_N]^T \tag{9}$$

where N will likely differ from K_{vis}. Also, the entries of $\mathbf{z}$ are not mapped to the VAs. The evaluation of the proposed positioning algorithm will incorporate all of these imperfections by statistical modeling of $\mathbf{z}$ as presented in Section III.

Our goal is to estimate the unknown position of the receiver by the ambiguous and noisy range measurements in $\mathbf{z}$ only. Therefore it is necessary to model the range measurements with a likelihood function $p_{\mathbf{z}|\mathbf{p}}(\mathbf{z}|\mathbf{p})$, parametrized by the position vector. Since the individual range measurements z_i are independent, this joint likelihood is the product of the marginal (individual) likelihoods. The joint likelihood can thus be written as

$$p_{\mathbf{z}|\mathbf{p}}(\mathbf{z}|\mathbf{p}) = \prod_{i=1}^{N} p_{z_i|\mathbf{p}}(z_i|\mathbf{p}) \tag{10}$$

which implies that we need to find a proper statistical model for the z_i. A maximization of (10) with respect to $\mathbf{p}$ yields a maximum likelihood (ML) estimator of the position $\mathbf{p}$

$$\hat{\mathbf{p}}_{\mathrm{ML}} = \arg\max_{\mathbf{p}} p_{\mathbf{z}|\mathbf{p}}(\mathbf{z}|\mathbf{p}) \tag{11}$$

If we also have prior knowledge about the receiver's position, we can apply the maximum a-posteriori probability (MAP) estimate

$$\hat{\mathbf{p}}_{\mathrm{MAP}} = \arg\max_{\mathbf{p}} p_{\mathbf{p}}(\mathbf{p}) p_{\mathbf{z}|\mathbf{p}}(\mathbf{z}|\mathbf{p}) \tag{12}$$

where $p_{\mathbf{p}}(\mathbf{p})$ is the prior density. Such prior knowledge could be obtained when sequential estimation is used, where it corresponds to the results of the last estimation step. We will demonstrate results for both the ML and MAP estimation in this paper.

III. Statistical modeling

To perform the position estimation explained in the previous section, we need the measurement likelihood function $p_{\mathbf{z}|\mathbf{p}}(\mathbf{z}|\mathbf{p})$ to solve (11) and (12). Therefore we have to consider the statistical modeling of $\mathbf{z}$.

First, we consider that not each of the K VAs need to be visible. We do this by assigning visibility probabilities to the VAs, i.e. we define the vector $\mathbf{v}$ as

$$\mathbf{v} = [v_1, ..., v_K]^T \tag{13}$$

where each v_k denotes the probability that the k-th VA is visible. Furthermore, we account for the presence of unmatched, spurious range estimates in $\mathbf{z}$, which are due to imperfections in the MPC extraction process. This is done by defining that an entry z_i of $\mathbf{z}$ is from a VA with probability P_{VA}. For the MAP position estimator, we also need a prior distribution for the receiver's position. Therefore, we treat $\mathbf{p}$ as a random variable following a bivariate normal distribution with a mean equal to the true position $\mathbf{p}_{\text{true}}$

$$p_{\mathbf{p}}(\mathbf{p}) = \mathcal{N}(\mathbf{p}_{\text{true}}, \mathbf{I}\sigma_p^2) \tag{14}$$

where $\mathbf{I}$ is the identity matrix. With these definitions, we can setup the likelihood function to maximize.

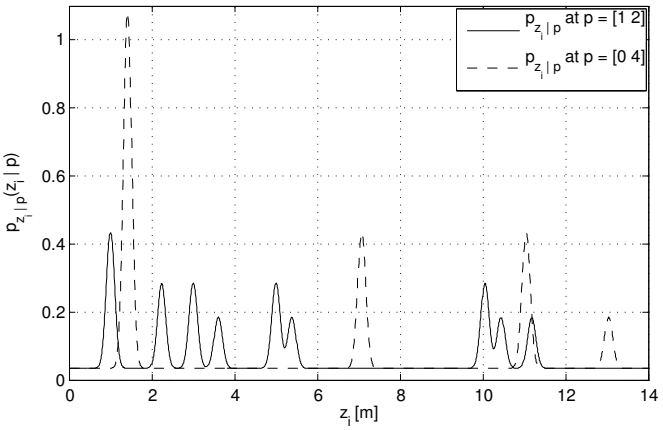

Fig. 2. Examples for the measurement likelihood function for two different positions $\mathbf{p}$. The solid curve is for $\mathbf{p} = [1, 2]^T$, the dashed one for $\mathbf{p} = [0, 4]^T$. In the latter, several modes have the same mean causing the overall likelihood to add up.

A. Measurement likelihood function without mapping

A crucial step in this positioning algorithm is the selection of proper statistical model for $p_{z_i|\mathbf{p}}(z_i|\mathbf{p})$. The joint likelihood function of the observation vector $\mathbf{z}$ can then be obtained using (10). A likelihood function for z_i that takes the above mentioned statistical parameters for $\mathbf{z}$ into account can be given as

$$\begin{aligned} p_{z_i|\mathbf{p}}(z_i|\mathbf{p}) &= P_{\mathrm{VA}} \frac{1}{\sum_{k=1}^{K} v_k} \sum_{k=1}^{K} v_k \mathcal{N}(||\mathbf{p} - \mathbf{p}_k||, \sigma_k^2) \\ &+ (1 - P_{\mathrm{VA}}) p_{z_i, \overline{\mathrm{VA}}|\mathbf{p}}(z_i|\mathbf{p}) \end{aligned} \tag{15}$$

where the first line is in principle a mixture density with K Gaussians, each one centered at the true distance to the k-th VA. These Gaussians are weighted by their visibility probabilities. So the first line corresponds to the sum of the probabilities that a certain z_i at a given position $\mathbf{p}$ is from one of the VAs.

In order to also account for possible spurious z_i that do not correspond to a VA, we also introduce the likelihood function $p_{z_i, \overline{\mathrm{VA}}|\mathbf{p}}(z_i|\mathbf{p})$ in (15). This function describes the PDF of an unmatched measurement z_i. It is controlled by the choice of $p_{z_i, \overline{\mathrm{VA}}|\mathbf{p}}(z_i|\mathbf{p})$, which we select as

$$p_{z_i, \overline{\mathrm{VA}}|\mathbf{p}}(z_i|\mathbf{p}) = \mathcal{U}[0, r_{\max}] \tag{16}$$

that is a uniform distribution between zero and a maximum value for the range measurement. This value is selected to be sufficiently larger than the largest possible distance to a VA. Note that according to this choice, unmatched measurements provide no information related to the position $\mathbf{p}$. However, (16) explicitly depends on $\mathbf{p}$ to show that other choices are possible, which might be an interesting subject for further research.

Figure 2 illustrates the measurement likelihood function (15) as a function of z for two fixed positions. The solid curve corresponds to a receiver position $\mathbf{p} = [1, 2]^T$. For this position, all of the K modes of the likelihood function are

distinguishable. Their location is equal to the distances of the K VAs. The heights of these modes are scaled according to the visibility model $\mathbf{v}$. The dashed line corresponds to the second position $\mathbf{p} = [0, 4]^T$, which is the upper left corner of the room. Here, several d_k are equal and so the corresponding modes in the likelihood function are not distinguishable. This reflects the possible uncertainty in mapping a z_i at a given position to a specific VA if the distances are equal.

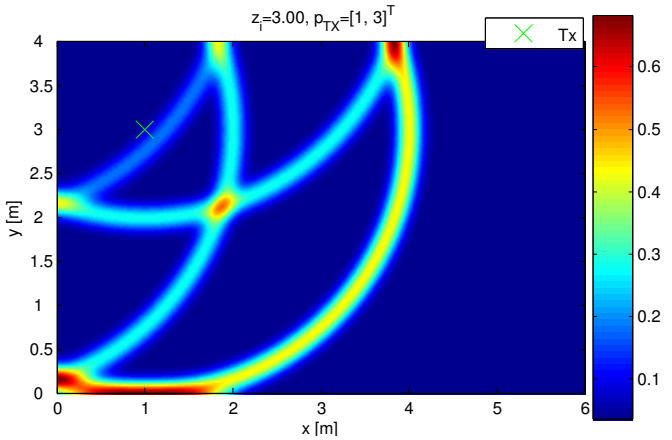

Fig. 3. Measurement likelihood function as a function of $\mathbf{p}$ for $z_i = 3$

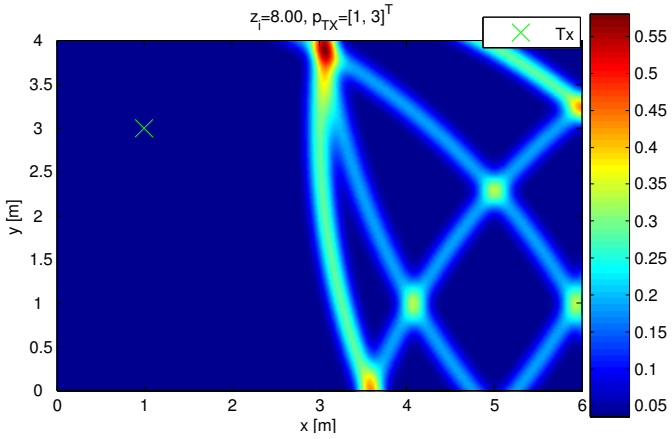

Fig. 4. Measurement likelihood function as a function of $\mathbf{p}$ for $z_i = 8$

Figures 3 and 4 provide alternative illustrations of the measurement likelihood function; $p_{z_i|\mathbf{p}}(z_i|\mathbf{p})$ is shown as a function of $\mathbf{p}$, with the range z_i fixed. In this way, the likelihood function corresponds to the objective function in the optimization problems (11) and (12). Looking at Fig. 3 for example we have $p_{z_i|\mathbf{p}}(z_i|\mathbf{p})$ for $z_i = 3$. We see the probabilities to be at a certain position $\mathbf{p}$ when this range measurement is observed. With a high probability, the receiver is on a circle with radius 3 around the transmitter, which corresponds to the direct signal path. With lower probabilities it is on circles corresponding to single and double reflections. The observations hold for Fig. 4 where $z_i = 8$. In this case, there is no possibility for the receiver to be at a position corresponding to the direct signal path.

Figures 3 and 4 also show a potential problem concerning the maximization of the likelihood function. Especially at the room boundaries, we observe high concentrations of the likelihood function around certain positions. This is due to the symmetry of the transmitter and the single reflection VAs with respect to the distance to these positions. We expect that these likelihood concentrations could lead to outliers, especially if the ML-estimator in (11) is directly used.

B. Measurement likelihood function with hard-decision mapping

In order to prevent the concentration of the likelihood at the room boundaries, we have to prevent the individual likelihoods in (15) from adding up whenever the distances to two or more VAs are similar. This summation of likelihood reflects the uncertainty in mapping an entry of $\mathbf{z}$ to a VA, which can not be done unambiguously. In principle, this prevents us from using the silver standard estimator from (6). We can however still use the associated likelihood functions for the r_k from (4) to find a statistical mapping for each z_i

$$p_{z_i|\mathbf{p}}(z_i|\mathbf{p}) = \max_k \left\{ p_{r_k|\mathbf{p}}(z_i|\mathbf{p}) \right\} \tag{17}$$

which selects the largest contribution from all the K VAs as the most probable likelihood for this z_i. However, if

$$p_{r_k|\mathbf{p}}(z_i|\mathbf{p}) < p_{z_i,\overline{\mathrm{VA}}|\mathbf{p}}(z_i|\mathbf{p}) \;\forall\; k \tag{18}$$

the range measurement z_i is considered an unmatched MPC. This however is a hard-decision mapping and completely ignores all information for z_i belonging to any other VA where the likelihood is maybe just slightly smaller. Note that this method of mapping does not prevent multiple z_i from being mapped to the same VA. This of course is a potential for future research.

The joint likelihood function $p_{\mathbf{z}|\mathbf{p}}(\mathbf{z}|\mathbf{p})$ is obtained in the same way as in (10) as a product of the marginal likelihoods. Position estimation is then done by maximizing this joint likelihood or the a-posteriori likelihood as in (11) and (12). The estimators obtained in this way will be denoted by $\hat{\mathbf{p}}_{\mathrm{ML,HD}}$ and $\hat{\mathbf{p}}_{\mathrm{MAP,HD}}$, respectively, where the subscript HD stands for hard decision.

C. Generation of measurement vectors

To perform performance simulations, we need to generate a set of observation vectors $\mathbf{z}$ that have the statistical properties that were outlined at the beginning of this section. This means that an individual measurement z_i has to be distributed according to (15). Hence, each z_i is either associated with a VA or a spurious observation not matched to a VA. The vector $\mathbf{z}$ is assembled from z_i which are generated according to these two cases.

In the first case, we have to take the visibility probabilities given in $\mathbf{v}$ into account. Using $\mathbf{v}$, we can calculate the PDF for the number of visible VAs K_{vis} and the expected value of K_{vis}

$$m_{\mathrm{VA}} = E\{K_{\mathrm{vis}}\} \tag{19}$$

Hence, K_{vis} can be drawn according to the visibility model. The z_i that are matched to a VA are then generated as noisy observations of the true distances to the corresponding images

$$z_{i,\mathrm{VA}} = d_i + w_i, \qquad w_i \sim \mathcal{N}(0, \sigma_i^2) \tag{20}$$

so in principle, the $z_{i,\mathrm{VA}}$ correspond to the entries of the vector $\tilde{\mathbf{r}}$ (see also (8)).

The second group of z_i are those not matched to a VA. With m_{VA} and the probability P_{VA} we can obtain the average number of non-VA MPCs as

$$m_{\overline{\mathrm{VA}}} = \frac{m_{\mathrm{VA}}}{P_{\mathrm{VA}}}(1 - P_{\mathrm{VA}}). \tag{21}$$

For modeling these MPCs we consider a PDF of their number which is triangular with a mean value equal to $m_{\overline{\mathrm{VA}}}$. The choice of this PDF is of course rather arbitrary and should be subject to careful examination in future research.

With these statistical models, we can use the proposed positioning algorithm from Section II, as the vectors $\mathbf{z}$ are generated in accordance to the model (15). Note that due to this statistical model, the vectors $\mathbf{z}$ that are generated for performance simulation also contain the cases where $K_{\mathrm{vis}} \in \{0, 1, 2\}$, which are cases that are not solvable unambiguously for any range-based positioning algorithm for two dimensions. Simulation results are presented in the next section.

IV. Results

The statistical models from Section III can be used together with the positioning algorithm presented in Section II for performance simulations. Table I contains an overview over standard simulation parameters that were used. In the following, parameters are only explicitly mentioned if they deviate from these standard values.

TABLE I
STANDARD PARAMETERS FOR SIMULATION MODEL

Parameter	Note	Standard value
Room dim.		6 m x 4 m
σ_k	Range estimate std. deviation	0.1 m $\forall\ k$
v_k	Visibility of images: LOS,	0.8 for $k = 1$
	single reflections,	0.5 for $2 \leq k \leq 5$
	double reflections	0.3 for $6 \leq k \leq 9$
P_{VA}	Prob. that a z_i is from an image	0.5
m_{p}	Position prior mean	$\mathbf{p_{true}}$
σ_{p}	Position prior std. deviation	1 m

Figures 5 and 6 show some samples from the position estimates for $\hat{\mathbf{p}}_{\mathrm{ML}}$ and $\hat{\mathbf{p}}_{\mathrm{MAP}}$ as well as for $\hat{\mathbf{p}}_{\mathrm{ML,HD}}$ and $\hat{\mathbf{p}}_{\mathrm{MAP,HD}}$, respectively, where the geometry from Fig. 1 is used. It seems that $\hat{\mathbf{p}}_{\mathrm{ML}}$ suffers from concentrated outliers at the top and bottom room boundaries, which is avoided by $\hat{\mathbf{p}}_{\mathrm{ML,HD}}$. In general, the MAP estimators exhibit much less outliers which is of course due to the prior knowledge. Figures 7 and 8 are logarithmic histograms for the position estimates from $\hat{\mathbf{p}}_{\mathrm{ML}}$ and $\hat{\mathbf{p}}_{\mathrm{ML,HD}}$ for 10^4 trials. They also confirm that $\hat{\mathbf{p}}_{\mathrm{ML,HD}}$ is useful in terms of its original motivation of

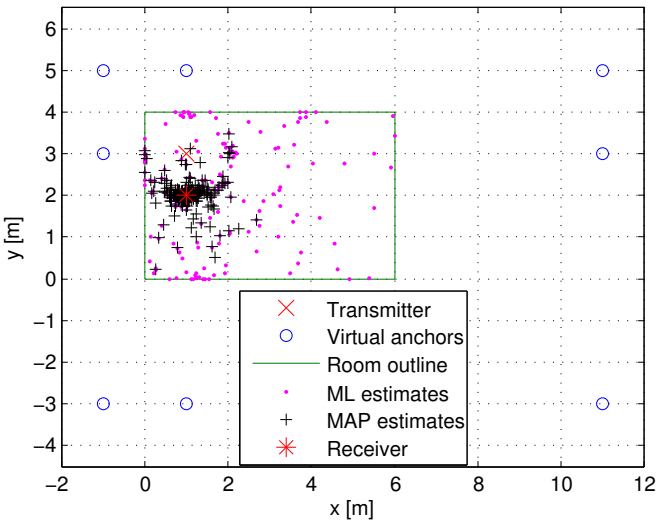

Fig. 5. Position estimates (300 points) for $\hat{\mathbf{p}}_{\mathrm{ML}}$ (magenta dots) and $\hat{\mathbf{p}}_{\mathrm{MAP}}$ (black plus signs) estimation based on (15) and standard simulation parameters.

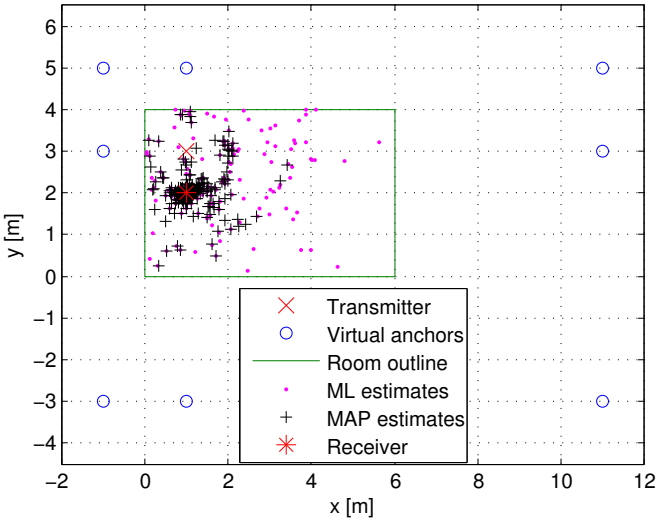

Fig. 6. Position estimates (300 points) for $\hat{\mathbf{p}}_{\mathrm{ML,HD}}$ (magenta dots) and $\hat{\mathbf{p}}_{\mathrm{MAP,HD}}$ (black plus signs) estimation based on (17) and standard simulation parameters.

preventing the adding up of the range likelihoods at the room boundaries.

To obtain a more general description of the positioning performance we define the absolute position error $\mathrm{Err}_{\hat{\mathbf{p}}}$ as

$$\mathrm{Err}_{\hat{\mathbf{p}}} = ||\mathbf{p}_{\mathrm{true}} - \hat{\mathbf{p}}|| \tag{22}$$

and estimate its CDF from the simulation data. A CDF of the error for standard parameters and all the position estimators introduced can be seen in Fig. 9 for 150 receiver positions on a rectangular, equally-spaced grid within the room. The grid spacing is 40 cm and the outermost positions are placed 20 cm within the walls. For $\hat{\mathbf{p}}_{\mathrm{MAP}}$, about 80% of all estimates are within 50 cm accuracy. The estimator $\hat{\mathbf{p}}_{\mathrm{ML}}$ shows a degraded performance, which is due to outliers that are mostly coupled

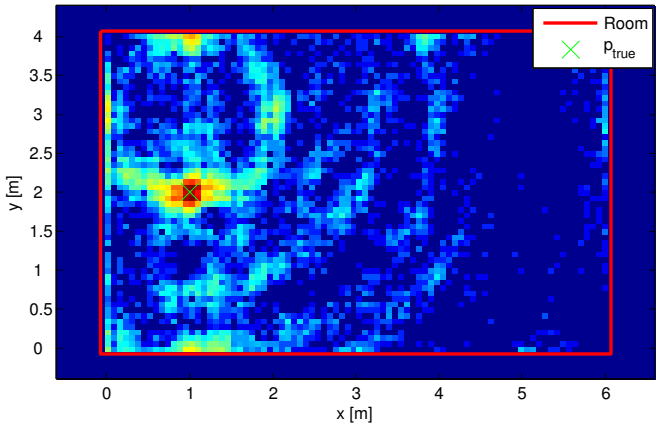

Fig. 7. Logarithmic histogram of the position estimates using $\hat{\mathbf{p}}_{\mathrm{ML}}$, which shows the concentration of outliers at the top and bottom room boundaries.

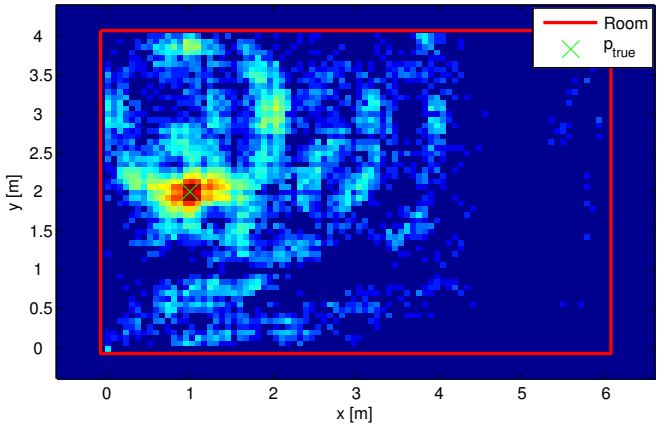

Fig. 8. Logarithmic histogram of the position estimates using $\hat{\mathbf{p}}_{\mathrm{ML,HDM}}$. The outliers at the top and bottom room boundaries are removed, but there are additional ones closer to the true position.

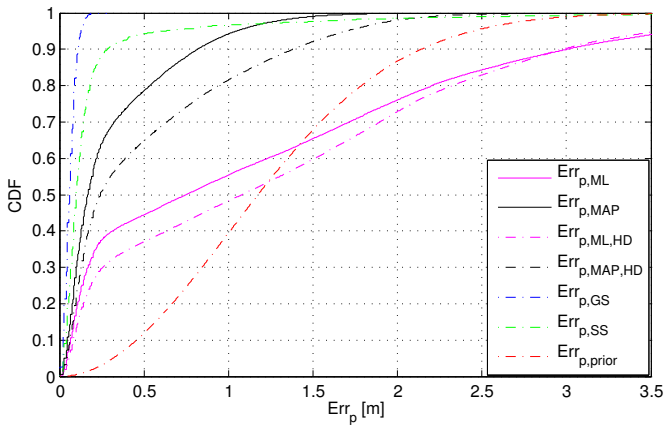

Fig. 9. Estimated CDF of the position error $\mathrm{Err}_{\hat{\mathbf{p}}}$ for all estimators considered and the position prior for comparison. The CDF shown is obtained using 150 positions on a rectangular equally-spaced grid across the room using the standard simulation parameters from Table I.

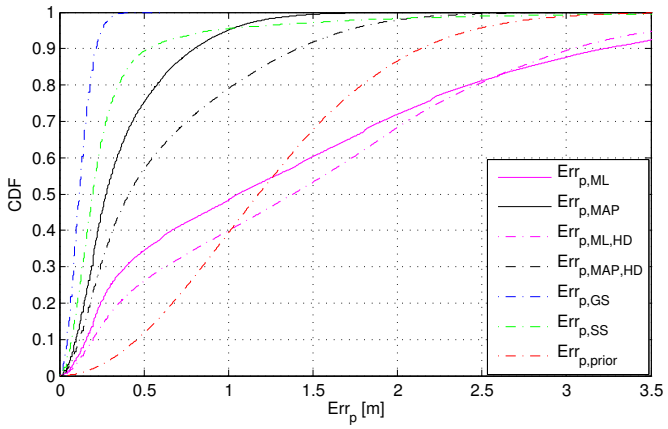

Fig. 10. Estimated CDF of the position error $\mathrm{Err}_{\hat{\mathbf{p}}}$ for all estimators considered and the position prior for comparison. The range measurement standard deviation is increased to $\sigma_k = 0.2$ m $\forall$ k in this plot.

to the uncertainty and ambiguity in the mapping of the z_i to the VAs. This is confirmed by the superior performance of the silver standard estimator that is shown for comparison. In general, the estimators $\hat{\mathbf{p}}_{\mathrm{ML}}$ and $\hat{\mathbf{p}}_{\mathrm{MAP}}$ have a better performance than the variants using hard-decision mapping.

The influence of noise on the range estimates to the virtual images of the transmitter are shown in Fig. 10. It can be observed that an increase of σ_k to 20 cm does not result in a dramatic increase of the position error at least for the MAP estimator.

Fig. 11 shows the performance CDFs when $P_{\mathrm{VA}} = 0.9$ which corresponds to a reliable MPC-extraction algorithm. For the standard setup we chose a rather pessimistic value of $P_{\mathrm{VA}} = 0.5$. It can be observed that a higher P_{VA} can highly increase the performance of the proposed algorithms. The MAP-estimators come close to the silver standard in this case.

The influence of the visibility of the VAs is shown in Fig. 12, where $\mathbf{v}$ has been changed to reflect a worse visibility (see caption). It is interesting that $\hat{\mathbf{p}}_{\mathrm{SS}}$ and the $\hat{\mathbf{p}}_{\mathrm{ML}}$ are degraded much more than $\hat{\mathbf{p}}_{\mathrm{MAP}}$. This is probably due to the availability of prior knowledge in $\hat{\mathbf{p}}_{\mathrm{MAP}}$. The high influence of the number of visible VAs is also confirmed by Fig. 13, where the mean position error for 10^4 trials at the receiver position $\mathbf{p}_{\mathrm{true}} = [1, 2]^T$ is shown as a function of the number of visible VAs K_{vis} and the number of unmatched entries in $\mathbf{z}$, denoted by K_{nonVA}. The former has more influence on the performance, as the mean error decreases with the number of visible VAs more rapidly than it increases with the number of unmatched z_i. For the MAP estimator, this effect is not as strong as for the ML estimator, because the prior knowledge effectively decreases the number of outliers.

V. Conclusions and Future Work

It has been shown that the proposed indoor positioning algorithm based on virtual anchors and ultra-wideband signals works in principle and is a promising candidate for robust indoor localization. Especially the MAP estimator shows a good performance, which is robust with respect to impairments

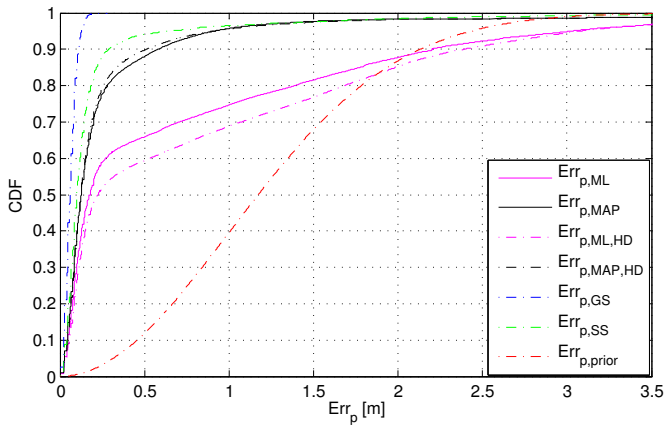

Fig. 11. Estimated CDF of the position error $\mathrm{Err}_{\hat{\mathbf{p}}}$ for all estimators considered and the position prior for comparison. P_{VA} is set to 0.9 to show the performance when an accurate MPC-extraction is used.

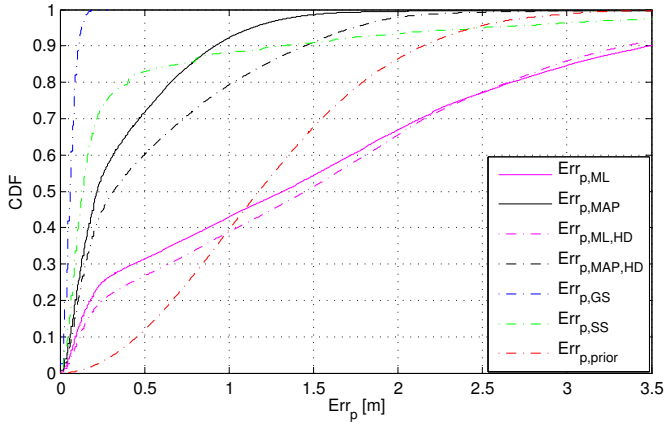

Fig. 12. Estimated CDF of the position error $\mathrm{Err}_{\hat{\mathbf{p}}}$ for all estimators considered and the position prior for comparison. The visibility model is changed to $v_k = 0.5, k = 1$ (direct path), $v_k = 0.4, k = 2, ..., 5$ (single reflections) and $v_k = 0.2, k = 6, ..., 9$ (double reflections) to reflect bad visibility conditions.

like bad visibility or increased range measurement noise. A key problem is the mapping of measurements to the virtual anchors, for which a first basic scheme has been introduced.

Future work will include the improvement of the mapping scheme, as we expect that it can lead to an improvement of the performance in principle. We will address the problem of possible multiple mappings of range measurements to one virtual anchor. Of course also the task of MPC extraction from the CIR deserves further attention, as its influence on the positioning algorithm has been shown to be crucial.

We will also consider movement of the receiver, where we will perform state-space estimation of the receiver node's position in order to exploit the temporal correlation of the positions. Techniques like Kalman- or particle filters could be employed for this task. Also multiple receivers and cooperative localization can be taken into account.

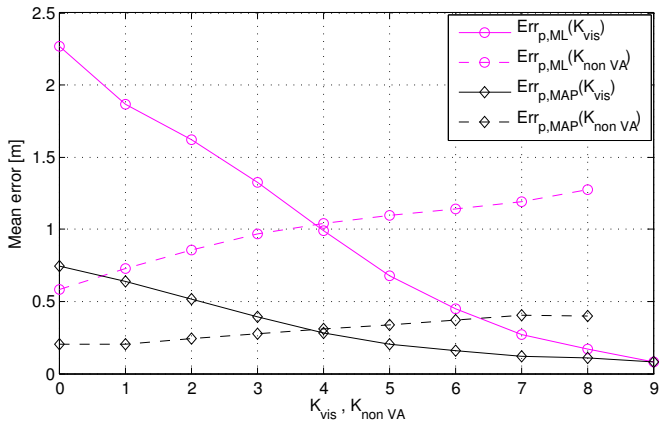

Fig. 13. Mean position error as a function of the number of visible images K_{vis} and non-image MPCs K_{nonVA} for $\hat{\mathbf{p}}_{\mathrm{ML}}$ and $\hat{\mathbf{p}}_{\mathrm{MAP}}$.

REFERENCES

[1] Y. Qi, H. Kobayashi, and H. Suda, "Analysis of wireless geolocation in a non-line-of-sight environment," *IEEE Trans. Wireless Commun.*, vol. 5, no. 3, pp. 672–681, Mar. 2006.

[2] S. Gezici, H. Kobayashi, and H. Poor, "Nonparametric non-line-of-sight identification," in *IEEE Vehicular Technology Conference, VTC*, vol. 4, Oct. 2003, pp. 2544–2548.

[3] J. Borras, P. Hatrack, and N. B. Mandayam, "Decision theoretic framework for nlos identification," in *Proc. 48th IEEE Vehicular Technology Conference VTC 98*, vol. 2, May 18–21, 1998, pp. 1583–1587.

[4] M. Heidari, N. A. Alsindi, and K. Pahlavan, "UDP identification and error mitigation in ToA-based indoor localization systems using neural network architecture," *IEEE Trans. Wireless Commun.*, vol. 8, no. 7, pp. 3597–3607, Jul. 2009.

[5] T. Deissler and J. Thielecke, "Feature based indoor mapping using a bat-type UWB radar," in *Proc. IEEE International Conference on Ultra-Wideband ICUWB 2009*, Sep. 9–11, 2009, pp. 475–479.

[6] S. Gezici, Z. Tian, G. B. Giannakis, H. Kobayashi, A. Molisch, H. V. Poor, and Z. Sahinoglu, "Localization via ultra-wideband radios: a look at positioning aspects for future sensor networks," *IEEE Signal Processing Mag.*, vol. 22, no. 4, pp. 70– 84, Jul. 2005.

[7] A. Molisch, "Ultra-wide-band propagation channels," *Proc. IEEE*, vol. 97, no. 2, pp. 353–371, Feb. 2009.

[8] Y. Qi and H. Kobayashi, "A unified analysis for Cramer-Rao Lower Bound for non-line-of-sight geolocation," in *36th Annual Conference on Information Sciences and Systems*, Mar. 2002.

[9] B. Fleury, M. Tschudin, R. Heddergott, D. Dahlhaus, and K. Ingeman Pedersen, "Channel parameter estimation in mobile radio environments using the SAGE algorithm," *IEEE J. Select. Areas Commun.*, vol. 17, no. 3, pp. 434–450, Mar. 1999.

[10] R. J.-M. Cramer, M. Z. Win, and R. A. Scholtz, "Evaluation of an ultra-wide-band propagation channel," *IEEE Trans. Antennas Propagat.*, vol. 50, no. 5, pp. 561–570, May 2002.